Neurocomputational account of how the human brain decides when to have a break

Florent Meyniel[a,b,c], Claire Sergent[b,c,d], Lionel Rigoux[a,b,c], Jean Daunizeau[a,b,c,e], and Mathias Pessiglione[a,b,c,e,1]

[a]Motivation, Brain and Behavior Laboratory, [d]Physiological Investigations of Clinical Normal and Impaired Cognition Laboratory, [e]Centre de NeuroImagerie de Recherche, [b]Brain and Spine Institute, Hôpital de la Pitié-Salpêtrière, 75013 Paris, France; and [c]Centre National de la Recherche Scientifique Unité Mixte de Recherche 7225, Institut National de la Santé et de la Recherche Médicale Unité Mixte de Recherche 975, Université Pierre et Marie Curie–Paris 6, 75005 Paris, France

Edited by Marcus E. Raichle, Washington University in St. Louis, St. Louis, MO, and approved December 11, 2012 (received for review July 12, 2012)

No pain, no gain: cost–benefit trade-off has been formalized in classical decision theory to account for how we choose whether to engage effort. However, how the brain decides when to have breaks in the course of effort production remains poorly understood. We propose that decisions to cease and resume work are triggered by a cost evidence accumulation signal reaching upper and lower bounds, respectively. We developed a task in which participants are free to exert a physical effort knowing that their payoff would be proportional to their effort duration. Functional MRI and magnetoencephalography recordings conjointly revealed that the theoretical cost evidence accumulation signal was expressed in proprioceptive regions (bilateral posterior insula). Furthermore, the slopes and bounds of the accumulation process were adapted to the difficulty of the task and the money at stake. Cost evidence accumulation might therefore provide a dynamical mechanistic account of how the human brain maximizes benefits while preventing exhaustion.

accumulation model | combined fMRI–MEG | decision making | effort/benefit trade-off | fatigue

Shall we have a break? The question of when we should stop ongoing work and when we should resume work again has to be solved every day. The problem can be reduced to a trade-off between the costs and benefits of effort exertion, which has been extensively investigated in the decision-making literature (1–4). However, standard decision theory only considers the question of whether to engage an action at a specific time point and does not account for the temporal dynamics of effort allocation. The temporal dynamics are difficult to determine beforehand because prior information about costs is usually limited. For instance, when people have to move a refrigerator up some stairs, they rarely decide in advance the number and duration of breaks. Although central for understanding high-level control of behavior, the issue of how the human brain monitors effort production online so as to make decisions about breaks is virtually unexplored.

William James (p. 323 in ref. 5) provided insightful intuitions about the underlying mechanisms: "Ordinarily, we stop when we meet the first effective layer, so to call it, of fatigue.... But, if an unusual necessity forces us to press onward, a surprising thing occurs. The fatigue gets worse up to a certain critical point, when gradually or suddenly it passes away.... We have evidently tapped a level of new energy." According to James, writing in the early 20th century, "psychologists ignore (this) conception altogether"; a century later, we intended to take it seriously. We retained three key features of James' conception: (*i*) there is a signal analog to fatigue that accumulates during effort exertion, (*ii*) the decision to stop is triggered by the signal reaching an upper bound, and (*iii*) the bound can be shifted depending on circumstances. To explain not only effort but also rest termination, we added the hypothesis that the same signal triggers the decision to resume work when reaching a lower bound.

The first aim of the present studies was to examine whether such signal, with both the waning and waxing components, is indeed represented in the human brain. We called this signal "cost evidence" to avoid making any strong assumption about how it relates to conscious subjective sensations such as fatigue or pain. This appellation also has the advantage of drawing an explicit link with both the literature on cost-based decision making (1–4) and the literature on evidence accumulation in the perceptual domain (6, 7). We note, however, that our signal is more complex than in classical perception studies, because it includes not only the accumulation but also the dissipation process. The second aim was to uncover how the putative cost evidence signal would be adapted to expected benefit and task difficulty, so as to maximize payoff while preventing exhaustion. In particular, we tested James' idea that motivation can push back the bounds against alternative models where it plays on accumulation slopes.

To investigate the process of cost evidence accumulation, we developed a paradigm where subjects are free to exert or not exert an effort over a long period (30 s). The paradigm was adapted from previous experiments that demonstrated the implication of the ventral striato-pallidal complex in incentive motivation, i.e., in energizing behavioral performance as a function of the reward at stake (8, 9). The task (Fig. 1) involves participants squeezing a handgrip to win a given amount of money, which was manipulated to vary the expected benefit of effort exertion. The key difference to previous tasks is that the payoff was proportional to the time spent above a given force level, which was manipulated to vary the cost of effort exertion. Thus, we had two orthogonal factors forming a three by three design: monetary incentive (*I*: 10, 20, or 50 cents) and effort difficulty (*D*: 70%, 80%, or 90% of the subject's maximal force). The incentive was displayed before each trial but the difficulty was not made explicit, such that subjects had to experience cost and adjust their behavior online.

We first examined at the behavioral level how these factors impacted the free parameters of the accumulation model: accumulation slope during effort (*Se*), dissipation slope during rest (*Sr*), and amplitude between bounds (*A*). Then we used two complementary functional neuroimaging techniques to search for brain activity signaling cost evidence: functional magnetic resonance imaging (fMRI) for an accurate localization of the putative cost evidence signal and magnetoencephalography (MEG) for a precise characterization of its temporal dynamics.

Results

Behavioral Results. Grip force was analyzed conjointly for the two groups who participated in the fMRI ($n = 19$) and MEG ($n = 19$) studies, because they exhibited similar behavior. As expected, subjects alternated periods of rest and effort in the course of a trial (see example in Fig. 2*A*). The duration of every single effort and rest period (not the total over the trial) was extracted to assess incentive and difficulty effects. Incentives significantly

Author contributions: F.M. and M.P. designed research; F.M. performed research; L.R. contributed new reagents/analytic tools; F.M., C.S., J.D., and M.P. analyzed data; and F.M. and M.P. wrote the paper.

The authors declare no conflict of interest.

This article is a PNAS Direct Submission.

[1]To whom correspondence should be addressed. E-mail: mathias.pessiglione@gmail.com.

This article contains supporting information online at www.pnas.org/lookup/suppl/doi:10.1073/pnas.1211925110/-/DCSupplemental.

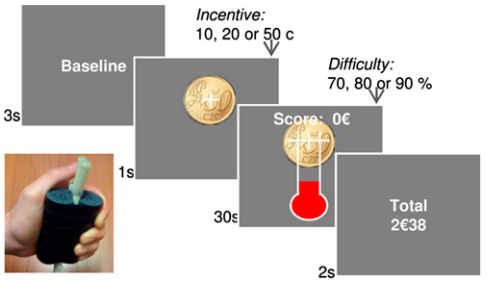

Fig. 1. Task. The illustrated screenshots were successively presented every trial. When the thermometer image was displayed, participants had to squeeze a handgrip to win as much money as possible. Subjects were provided online feedback on force level and cumulative payoff. The payoff was only increased when force level was above the target bar, at a constant rate proportional to the monetary incentive. Two factors were manipulated over trials: the incentive (10, 20, or 50 cents), which was explicitly indicated as a coin image, and the difficulty, i.e., the force required to reach the target bar (70%, 80%, or 90% of maximal force), which remained implicit. The last screen indicated the money won so far, summed over all preceding trials.

affected the duration of both effort [$F_{(2,72)} = 25.3$; $P = 1.6 \times 10^{-6}$] and rest [$F_{(2,72)} = 25.2$; $P = 4.9 \times 10^{-7}$] periods, whereas difficulty only affected effort duration [$F_{(2,72)} = 42.8$; $P = 2.8 \times 10^{-12}$], not rest duration [$F_{(2,72)} = 0.1$; $P = 0.86$]. There was no significant incentive by difficulty interaction, neither for effort [$F_{(4,144)} = 1.7$; $P = 0.18$] nor for rest [$F_{(4,144)} = 1.4$; $P = 0.26$] duration. Thus, subjects spent more time squeezing and less time resting for higher incentives, and less time squeezing with higher difficulty (Fig. 2*B*).

We then examined which free parameters of the accumulation model best explained the observed effects on effort and rest durations (effort time, $Te = A/Se$, and rest time, $Tr = A/Sr$). Each free parameter (*Se*, *Sr*, and *A*) was written as a linear combination of the experimental factors (*I* and *D*), for instance $A = A_{\text{mean}} + A_I{}^*I + A_D{}^*D$. Note that we did not include any interaction term because there was no significant incentive by difficulty interaction in our data. Each of the three parameters could in principle be modulated or not modulated by each of the two factors, leading to a total of 64 linear models (Fig. S1, *Upper*). Only 20 of the 64 possible models could a priori produce the observed behavioral pattern. These 20 models were estimated and compared using Bayesian model selection (BMS). The same best model was identified separately in the fMRI and MEG groups, with exceedance probability xp = 0.97 and xp = 0.84, respectively (Fig. S1, *Lower*). In this model, incentives play on both *Sr* and *A*—they accelerate cost evidence dissipation during rest and expend the amplitude between bounds—whereas difficulty only plays on *Se*—only accelerates cost evidence accumulation during effort.

fMRI Results. We used fMRI during task performance to assess (*i*) whether some brain activity is correlated with cost evidence accumulation during effort and dissipation during rest and (*ii*) whether the amplitude of this putative brain signal is modulated by incentives.

We estimated a first general linear model (GLM1) including cost evidence as a parametric modulator of neural activity at every time point, with constant amplitude throughout all conditions (Fig. 3*A*). This cost evidence signal was significantly expressed (surviving both voxel- and cluster-wise whole-brain correction) in the bilateral posterior insula (secondary somatosensory cortex SII) and the ventromedial thalamus (Fig. 3*B* and Table S1). These two brain regions are considered components of the so-called pain matrix and more generally of the proprioception network (10, 11). We extracted them together to form a single region of interest (ROI) that we used in all of following analyses. Note that the same maps were obtained whether or not the exerted force level was included as an additional regressor in the GLM (compare Tables S1 and S2).

Three additional GLMs were built to account for amplitude modulation by incentives with changes in the upper bound (GLM2), lower bound (GLM3), or both bounds (GLM4). BMS analysis (Fig. 3*C*) indicated that the activity extracted from the ROI was best explained (with xp > 0.99) by GLM including amplitude modulation (GLM2-4 versus GLM1), i.e., GLMs that were not used to identify the ROI. Among the three possible modulations, changing both bounds (as illustrated in Fig. 3*A*) was the most probable (xp > 0.96 for GLM4). Thus, fMRI data revealed that proprioceptive regions continuously signal cost evidence over effort and rest periods. Additionally, they showed that the two bounds triggering effort cessation and return are moved apart when incentives are increased, an effect that could not be inferred from behavioral data.

MEG Results. We used MEG to confirm the conclusions drawn from the fMRI study with a reverse approach: instead of a model-driven approach showing that a theoretical signal fits brain activity, we followed a data-driven approach to show that brain activity fulfills theoretical predictions. More specifically we assessed (*i*) whether scalp activity arising from the ROI sources was ramping up and down during effort and rest periods and (*ii*) whether incentive and difficulty effects on bounds and slopes conformed to the model optimized on behavioral and fMRI data.

MEG time series were epoched into behaviorally defined rest and effort periods, which were resampled to a same duration and averaged over conditions and subjects. The principal component analysis (PCA) performed on this grand average revealed that

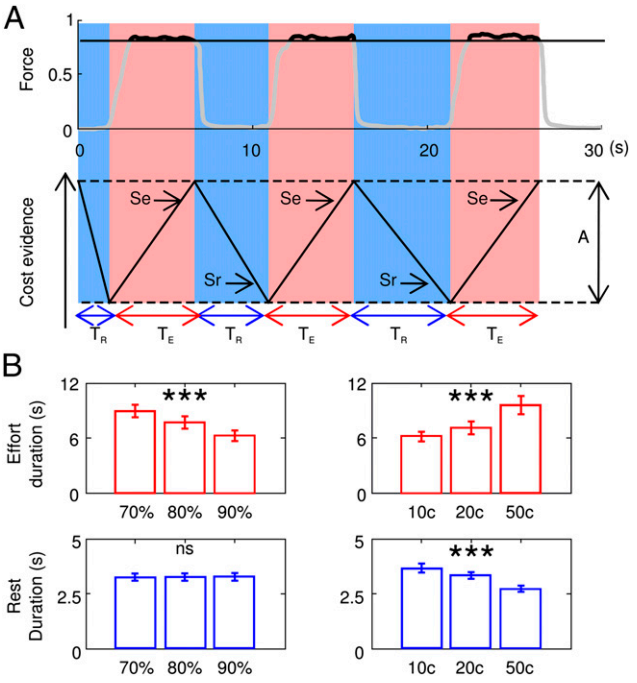

Fig. 2. Behavioral results. (*A*) Example recording of the force exerted during one trial. Three effort (red shading) and three rest (blue shading) epochs could be defined. Force level is shown in black (not gray) when rewarded, i.e., when above the target level (here, 80% of maximal force). The theoretical cost evidence that was hypothesized to underpin effort production is shown below. *A*, amplitude between bounds; *Sr*, dissipation slope during rest; *Se*, accumulation slope during effort; *Te*, effort time; *Tr*, rest time. (*B*) Average data pooled over the MEG and fMRI studies, sorted by incentive and difficulty levels. The bars are mean effort and rest epoch durations, and error bars are the intersubject SEs. Significance of group-level ANOVA main effects: ***$P < 0.0005$, **$P < 0.005$, *$P < 0.05$.

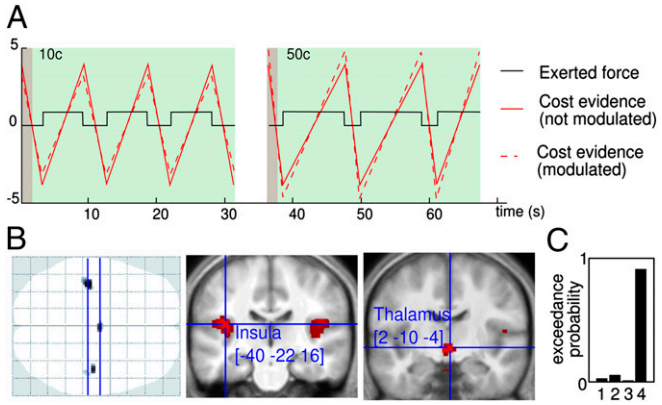

Fig. 3. fMRI results. (*A*) Example of two successive trials with the corresponding cost evidence modeled for fMRI data analysis. The green and gray shading indicate incentive display and effort exertion periods. The incentive was 10 cents in the left trial and 50 cents in the right trial. The exerted force is shown in black and the cost evidence in red. Two alternative cost evidence regressors are illustrated: one with a constant amplitude (solid line) and one with both bounds modulated by the incentive (dashed line). (*B*) Neural correlates of cost evidence. The statistical parametric maps show brain regions where activity was significantly correlated with cost evidence with constant amplitude. Statistical threshold was set at $P < 0.05$ with voxel-wise (axial projection plan on the left) or cluster-wise (coronal slices on the right) family-wise error correction for multiple comparisons over the entire brain. The coronal slices were taken along the planes indicated by the blue lines on the glass brain. The [*x y z*] peak coordinates refer to the Montreal Neurological Institute (MNI) space. (*C*) Modulation of cost evidence amplitude. The bar graph represents the result of a Bayesian model selection comparing the fit of different cost evidence regressors to the activity recorded in the significant clusters shown on slices (bilateral posterior insula and ventromedial thalamus). The cost evidence regressors differed on which bound was impacted by incentives: 1 = none, 2 = upper bound, 3 = lower bound, and 4 = both bounds.

both effort and rest periods were dominated by ramping activity (Fig. 4*A*). Indeed, the first components were linear variations that accounted for most of the signal variance (91% for effort and 72% for rest periods). The sources of these first components were reconstructed subject-wise with a minimum-norm procedure, either unconstrained or informed by setting priors on the fMRI-based ROI. BMS showed that the reconstruction using the anatomical priors had a much higher exceedance probability (xp = 0.90 for effort and xp = 0.94 for rest). Thus, the effort and rest ramping signals that dominated scalp activity were most likely to arise from the same sources: the ROI identified with fMRI. This is consistent with the idea that these regions (posterior insula and ventromedial thalamus) generate an accumulation signal throughout task performance.

We then returned to scalp raw time series (no resampling and averaging) and estimated accumulation and dissipation slopes using linear regression for every single effort and rest epoch on each channel (Fig. 4*B*). In each subject, slopes were averaged over epochs and conditions, for effort and rest separately. The sources of slope topography were reconstructed subject-wise, using either unconstrained or informed minimum-norm procedure as above. The BMS showed again that including fMRI-based priors largely improved reconstruction plausibility (xp = 0.75 for effort and xp = 0.94 for rest).

Individual reconstruction matrices were then used to estimate accumulation and dissipation slopes in the source space for each epoch and subject. The variations of these slopes were fitted with a linear model including incentive and difficulty levels as regressors. Incentives affected both accumulation slope during effort and dissipation slope during rest ($P < 0.004$ and $P < 0.008$, respectively), whereas difficulty only impacted accumulation, not dissipation slope ($P < 4 \times 10^{-6}$ and $P > 0.9$, respectively). Thus, the modulations identified from behavior (incentive increasing *Sr* and difficulty increasing *Se*) were confirmed and an additional modulation (incentive decreasing *Se*) was revealed. The effect of this additional modulation is to prolong effort periods for higher incentives, which was so far entirely imputed to larger amplitude between bounds.

To assess whether the amplitude of the accumulation signal identified in MEG activity was modulated, we fitted a single V shape to every contiguous rest–effort duplet. Regression coefficients were taken as amplitude estimates and were submitted to the same analysis as slopes. The source reconstruction for these amplitudes as well was much more plausible when including the fMRI-based ROI as priors (xp = 0.91). The linear regression

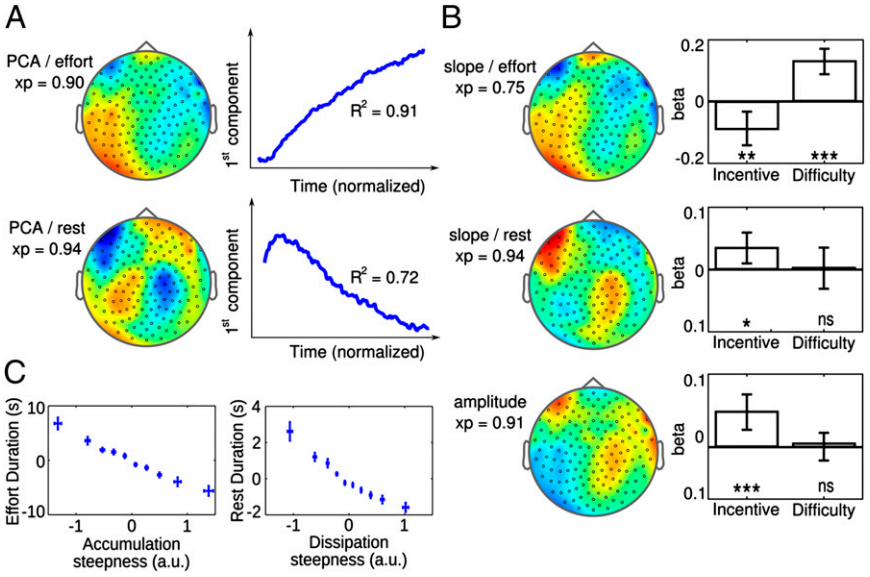

Fig. 4. MEG results. (*A*) PCA performed on average activity for effort and rest epochs separately. The scalp topography, time series, and proportions of variance explained (R^2 statistics) correspond to the first component. (*B*) Regression analysis performed on every single event to estimate accumulation slope (by fitting a line to rest and effort epochs separately) and amplitude (by fitting a V shape to two consecutive rest and effort epochs). For each analysis, the scalp topography shows the slopes and amplitudes averaged over trials and subjects. The bar graph represents the coefficients (β values) obtained for the two experimental factors (incentive and difficulty) with a linear regression model fitted on the slopes and amplitudes reconstructed within the regions identified with fMRI. Error bars are intersubject 5% confidence intervals. Significance of group-level *t* tests: $***P < 0.0005$, $**P < 0.005$, $*P < 0.05$. For each scalp topography, the xp value denotes the exceedance probability of the source reconstruction model that included as priors the regions identified with fMRI. (*C*) Correlation between residual durations and accumulation or dissipation steepness, obtained by regressing out incentive and difficulty effects. Durations were defined from behavioral data and slopes from MEG data reconstructed in the source space. Effort duration was plotted against accumulation steepness (*Left*) and rest duration against dissipation steepness (*Right*). For illustration, data were binned into deciles in every subject. The dots represent intersubject means ± SEs for the 10 bins. Note that we use steepness instead of slope for the accumulation signal (power) reconstructed in the source space because it is not signed.

performed on amplitudes in the source space showed a significant increase with higher incentives but no significant modulation by difficulty ($P < 3 \times 10^{-4}$ and $P > 0.65$, respectively). Thus, MEG data revealed that incentives in fact affected all three parameters of the accumulation model (*Se*, *Sr*, and *A*), whereas the difficulty effect remained relatively specific (only impacting *Se*).

Additionally, we tested whether incentive and difficulty effects would also be observed across subjects. Between-subject correlations between mean durations and accumulation parameters replicated all four effects that were found to explain the modulation of behavior by incentive and difficulty levels (Fig. S2). Thus, subjects with greater effects on accumulation/dissipation slope or amplitude had greater effects on effort/rest duration.

The above analyses suggest that incentive and difficulty effects on effort and rest durations are underpinned by modulation of cost evidence accumulation slopes and bounds. However, a strong prediction of the model is that decisions to engage and terminate effort are triggered by the cost evidence signal reaching a predetermined threshold. This implies that effort and rest durations should be correlated with accumulation and dissipation slopes, respectively, even when the correlation induced by our experimental manipulation is removed. To assess this prediction, we regressed the variance related to incentive and difficulty levels out of the reconstructed signal and duration, and tested the correlation between residual steepness and duration (Fig. 4*C*). The correlation across trials was negative for every subject and for both effort and rest periods: the steeper the slope, the shorter the duration. Correlation coefficients were highly significant at the group level for both effort ($P = 1.4 \times 10^{-8}$) and rest periods ($P = 5.9 \times 10^{-11}$).

Taken together, fMRI and MEG findings demonstrated that cost evidence is indeed tracked in proprioceptive brain regions and that the impact of potential benefits on the accumulation process is more complex than suggested solely on the basis of behavior (see illustration in Fig. S3).

Discussion

We addressed the issue of how the human brain dynamically allocates effort over time, depending on costs and benefits. We found a brain signal that linearly accumulates cost evidence during effort production and dissipates at rest. The observed decisions to stop and restart effort production corresponded to this cost evidence signal reaching upper and lower bounds. We argue that such a mechanism is adaptive because, contrary to benefit estimates, cost estimates can be refined during the course of action, using the information about how much work has been effectively exerted.

In addition, it constitutes an application to the proprioception domain of the accumulation principle that has been implicated in other processes, such as visual perception (6, 7) or subjective valuation (12–14), and interpreted as a process extracting information from a noisy input. However, there are several important differences between standard perceptual evidence accumulation and the process investigated in our study. Here, the functional role of the accumulation process would consist in adjusting effort and rest durations, so as to maximize the payoff while avoiding the peripheral and central damages that can result from prolonged exercise (15–17). It remains unclear whether our accumulation signal reflects an integration process because we do not know the sensory input. It could be a stationary signal related to muscle contraction (i.e., force level), or a signal related to any metabolic or physiological variable that would itself fluctuate over effort and rest periods. Also, the question of how the accumulation signal is reinitialized for subsequent trials is generally not addressed, or at least not interpreted functionally, in perception studies. In our case, the dissipation process would have a functional significance: it would indicate when the body is available for the next effort, and hence when effort should be resumed to maximize benefits. Because of this dissipation, our cost evidence signal cannot be considered as reflecting a pure accumulation (which would only increase). One interpretation of the dissipation process is that the accumulation is leaky, meaning that the effort is progressively forgotten during rest. Another interpretation is that a control input is subtracted to the sensory input to reset the system. In any case, the global cost evidence signal could be interpreted in terms of predictive coding, as an estimate of exhaustion probability (i.e., temporal proximity).

This complex neural signal with precise spatiotemporal characteristics was identified with both fMRI and MEG using standard analytical tools, which validates the usual assumptions about the relationships between electromagnetic and hemodynamic activity (18–22). Due to its high temporal resolution, MEG brought evidence that the electromagnetic activity emitted by our regions of interest indeed followed the neural dynamics that was modeled and convolved with hemodynamic response to fit fMRI data. In addition, due to its high spatial resolution, fMRI confirmed that our theoretical cost evidence signal was indeed represented in proprioceptive brain regions. The sign of the correlation observed with fMRI, denoting a signal ramping up during effort and down during rest, favored an interpretation in terms of cost evidence accumulation. This was important because, in principle, balancing effort and rest could rely on a signal representing energy dissipation (i.e., the available resource), not cost accumulation (i.e., the expended resource).

Our interpretation was confirmed by the signal being encoded in regions pertaining to the pain matrix, such as the posterior insula and ventral thalamus (10, 11). More precisely, the main activation foci were located in the operculum parietale area 1, which has been implicated in high-order somatosensory processing, in connection with both the ventral thalamus and parietal network (23). The classical pain matrix additionally includes midcingulate regions (24, 25), which were also activated in relation to cost evidence in our results but slightly below the statistical threshold for significance. Interestingly, direct electrical stimulation of the posterior insula was shown to induce painful sensations (26). However, we cannot infer from brain localization alone that the cost evidence variable can be equated to a subjective pain sensation. Indeed, different functions have been assigned to this brain network and particularly to the posterior insula, such as the monitoring of bodily states (27–29).

Let us emphasize that the signal labeled here as cost evidence did not mirror the behavioral output. Its linear fluctuations, dipping when effort starts and peaking when effort ends, were decorrelated from the force produced, which followed a boxcar dynamics. Thus, contrary to the behavioral output, the cost evidence signal spanned the same range of values in effort and rest periods. We believe that the dissipation at rest arises from an active process rather than from a passive relaxation. This is because, at the beginning of trials when subjects had not yet squeezed the handgrip, the cost evidence signal was first brought down to the lower bound in anticipation of effort exertion. This resembles the motor readiness potential that is known to precede limb movements by a few seconds. However, this readiness potential has been localized in motor cortical areas and not in deep proprioceptive regions (30, 31). In addition, the complex modulation of our cost evidence signal by monetary incentives suggests that it is not merely related to motor output.

The model selected from our data suggests that difficulty and incentive levels have computationally distinct impacts on the accumulation process that underpins effort allocation. Task difficulty probably impacted the behavior on the fly, as it was not explicitly mentioned to subjects, whereas the effects of monetary incentives, which were explicitly indicated at trial start, could be regarded as a strategic adjustment. Consistently, difficulty effects specifically manifested as an increased accumulation rate during effort, leaving unchanged the dissipation rate during rest. This was related to the nontrivial behavioral observation that rest duration did not change with task difficulty.

Incentive effects were twofold: (*i*) they slowed accumulation and speeded dissipation of cost evidence and (*ii*) they moved the bounds within which cost evidence fluctuates. The first process

might reflect the intervention of an opponent motivation signal that would be continuously subtracted to cost evidence throughout effort and rest periods. This signal might come from brain regions involved in reward processing, or in the trade-off between reward and effort, such as the ventral striatum, the anterior cingulate cortex, or the ventromedial prefrontal cortex (9, 32, 33). The second process might implement the intuitive psychological phenomenon that, when motivated, we literally push back our limits, allowing our body to work closer from exhaustion. It could be explained by reward-related regions adjusting decision thresholds in regions that are downstream to the posterior insula in the chain leading to motor outputs. However, these speculative mechanisms that might adjust accumulation parameters to expected benefits would require further investigation.

Note that incentive effects argue against the possibility that the signal might encode money and not cost accumulation, because the slope observed during effort decreased, not increased, with higher incentives. These effects are also consistent with reports that placebo analgesia reduce insular and thalamic responses to pain stimulation (34), and therefore that the brain can indeed adjust the sensitivity of these regions depending on expectations. More generally, our conclusions are in line with the "central governor" model, which supposes an anticipatory regulation of exercise performance, as opposed to catastrophic models, which attribute performance cessation to homeostatic failure (35, 36). They extend the theory, which was meant to explain how athletes pace their running on a treadmill, to the problem of when people have breaks during work.

Thus, our findings provide empirical evidence supporting the intuition, partly specified by William James a century ago (5), that effort allocation might be controlled online using an accumulation signal reaching bounds. James formulated this idea in psychological terms based on his own introspection; here, we propose a paradigm that allows probing this psychological concept and we reveal a possible implementation at the neural level. The relationship between the two description levels remains to be specified: we have not established yet whether the cost evidence signal is related to what we subjectively perceive as fatigue or pain. Another unresolved issue is whether this signal is indeed causally involved in the decision to cease and resume effort production. Further experiments would be needed to address these remaining issues. For instance, analgesic treatments may help establish causal links between cost evidence accumulation, subjective pain, and online effort allocation.

Materials and Methods

See *SI Materials and Methods* for behavioral and imaging data acquisition settings.

Subjects. The study was approved by the Pitié-Salpétrière Hospital ethics committee. All subjects were recruited via e-mail within an academic database and gave informed consent before participation in the study. They were right-handed, between 20 and 30 y old, and had normal vision, no history of neurological or psychiatric disease, and no contraindication to MRI. Twenty subjects (eight males; age, 23.6 ± 0.6 y) were included in the fMRI study and 19 in the MEG study (eight males; age, 24.9 ± 0.7 y). One subject in the fMRI study was excluded from the analysis because of calibration issues. Subjects believed that the money won while performing the task would be their remuneration for participating, but eventually their payoff was rounded up to a fixed amount (100€).

Behavioral Task. Before starting task performance, we measured the maximal force for each hand, following published guidelines (37). Participants were verbally encouraged to squeeze continuously as hard as they could, until a line growing in proportion to their force reached a target displayed on a computer screen. Maximal force was defined as the average, over the last half of the squeezing period, of data points exceeding the median force. Then subjects were provided a real-time feedback about the force produced on the handgrip, which appeared as a fluid level moving up and down within a thermometer, the maximal force being indicated as a horizontal bar at the top. Subjects were asked to try outreaching the bar and state whether it truly corresponded to their maximal force. If not, the calibration procedure was repeated.

Task sessions included nine trials corresponding to the nine cells of the factorial design (three incentive by three difficulty conditions), which were presented in a random order. Subjects performed eight sessions in total, switching hands as instructed between sessions to avoid muscle exhaustion. After baseline measurement of the pressure at rest, each trial started by revealing the monetary incentive with a coin image (10, 20, or 50 cents) displayed for 1 s. Then subjects had 30 s to win as much money as possible. They knew that the payoff was proportional to both the incentive and the time spent above the target bar, which was always placed at the same height in the thermometer. The force needed to reach the bar (70%, 80%, or 90% of subject's maximal force), i.e., trial difficulty, was not indicated to subjects. Subjects only knew that task difficulty would vary across trials. They were provided with online feedback on both the exerted force (with a fluid level moving up and down within a thermometer) and the trial-wise cumulative payoff (with a counter displayed above the thermometer). The counter was only started when fluid level was above the target bar, with a rate proportional to the current incentive. The fluid had the same luminance as the background to avoid confounding force level with basic visual features. Each trial ended with a 2-s display of the session-wise cumulative payoff.

Behavioral Data Analysis. Effort onsets and offsets were identified offline with an algorithm using the same two criteria for all conditions: (*i*) force temporal derivative higher than 1 SD and (*ii*) force level lower (for effort onset) or higher (for effort offset) than half the maximal force. The first rest period started with coin presentation and the subsequent effort and rest periods were defined by force onsets and offsets. Effort and rest period durations were separately analyzed using a repeated-measure ANOVA (R software; Companion to Applied Regression library of John Fox, McMaster University, Hamilton, ON, Canada), with incentive and difficulty as factors of interest. The *P* values reported for these repeated-measure ANOVAs integrate the conservative Greenhouse–Geisser correction.

The accumulation model was formalized with the following observation equations: $Te = \frac{A}{Se}$; $Tr = \frac{A}{Sr}$ with $\begin{cases} A = A_{\text{mean}} + A_I I + A_D D \\ Se = Se_{\text{mean}} + Se_I I + Se_D D \\ Sr = Sr_{\text{mean}} + Sr_I I + Sr_D D, \end{cases}$

where cost evidence variations have an amplitude *A*, a slope *Sr* during rest and *Se* during effort; *Te* and *Tr* are the effort and rest period durations; *I* and *D* are the *z*-scored incentive and difficulty levels. Each experimental factor (incentive and difficulty) could in principle affect each free parameter (*A*, *Se*, and *Sr*). We used BMS to test whether each possible modulation (A_I, A_D, Se_I, Se_D, Sr_I, and Sr_D) was significant. There were $2^6 = 64$ possible models but only 20 combinations could a priori reproduce the three behavioral results: increased *Te* with incentive, decreased *Tr* with incentive, and decreased *Te* with difficulty (Fig. S1). These 20 models were inverted using a variational Bayes approach under the Laplace approximation (38, 39), implemented in a toolbox by Jean Daunizeau (available at http://sites.google.com/site/jeandaunizeauswebsite/). This algorithm not only inverts nonlinear models but also estimates their evidence, which represents a trade-off between accuracy (goodness of fit) and complexity (degrees of freedom) (40). The log-evidences estimated for each subject and model were submitted to a group-level random-effect analysis (41) using SPM8 (Statistical Parametric Mapping, Wellcome Department of Imaging Neuroscience, London, UK).

fMRI Data Analysis. All GLMs included realignment parameters as covariates of no interest to correct for movement artifacts. Regressors of interest were specified at the 125-ms scale, and convolved with the canonical hemodynamic response function (HRF) and its first temporal derivative. The GLM included two categorical regressors: one modeling coin display onset with a delta function and one modeling the entire session with a boxcar function. There were also two parametric regressors: one modulating coin display by its value (10, 20, or 50 cents) and one modeling cost evidence variation over the entire session. Cost evidence was continuously modeled over effort and rest periods defined from the behavior, with linear increases and decreases between constant minimum and maximum, and then *z*-scored. Thus, the parametric cost evidence regressor was ramping up and down, between positive and negative values, during task trial and put to zero between trials (Fig. 3*A*).

Regression coefficients were estimated at the subject level using the standard restricted minimum-likelihood (ReML) estimation implemented in SPM8. Individual linear contrasts of HRF regressors were then taken to a group-level random-effect analysis using one-sample *t* tests. Statistical thresholds corresponding to correction for multiple comparisons over the entire brain were determined using the randomization ($n = 10{,}000$ permutations) technique implemented in FSL (Centre for Functional MRI of the

Brain, Oxford, United Kingdom). Two thresholds were used: a voxel-wise family-wise error (FWE) rate of $P < 0.05$ and a cluster-wise FWE rate of $P < 0.05$ (defined for voxels surviving $P < 0.001$, uncorrected). The cost evidence regressor mapped onto three regions (bilateral posterior insula and ventromedial thalamus) that survived both voxel-wise and cluster-wise corrections. These three clusters formed at $P < 0.001$, uncorrected, were grouped together to form a single region of interest, which was used for all subsequent analyses.

Three other GLMs were built that differed only on the cost evidence regressor, which now had an amplitude modulated by incentives in the same proportion as the model optimized on behavior. This modulation could in principle rely on the upper bound only (GLM2), or the lower bound only (GLM3), or be shared between both bounds (GLM4). Variational Bayes estimation procedure implemented in SPM8 was used to estimate for each subject the GLM log-evidences, which were summed over all voxels included in the ROI. Individual log-evidences were then submitted to a group-level random-effect BMS to identify the most probable cost evidence model given the ROI activity.

MEG Data Analysis. For the PCA, MEG data were epoched into rest and effort periods, resampled to 1,250 points, and averaged over conditions. A PCA was computed on the grand average (over subjects) to estimate the R^2 statistic of each component for rest and effort periods, separately. PCAs were also computed in each subject to reconstruct the sources of the first component with SPM8, using a minimum-norm algorithm that could include or not include the fMRI-based ROI as priors. The best reconstruction method (with or without priors) was determined using group-level BMS (42).

For the slope and amplitude analyses, three regressions were performed on the scalp raw time series. A linear trend was first fitted separately on rest and effort epochs to estimate accumulation and dissipation slopes, respectively. Then a V shape was fitted on contiguous rest–effort epochs to estimate the signal amplitude. Sources of the mean slopes and amplitudes were reconstructed subject-wise using the same procedure as for PCA. The estimated scalp-to-source reconstruction matrices were then used to invert each epoch. Activity in the source space was rectified (absolute value), log-normal transformed, and averaged within the ROI. The resulting activity was analyzed using a linear model including three regressors: incentive (10, 20, 50) and difficulty (70, 80, 90) levels plus a constant. The significance of regression coefficients was estimated at the group level using a two-tailed t test.

ACKNOWLEDGMENTS. We thank A. Ducorps, C. Gitton, L. Hugueville, and V. Marchand-Pauvert for critical technical support with electrophysiological recordings; the Centre de NeuroImagerie de Recherche team for their help with fMRI recordings; T. Andrillon and R. Le Bouc for their help in behavioral pilots and data acquisition; and C. Tallon-Baudry for her comments on the MEG analysis. This study was funded by a Starting Grant from the European Research Council. F.M. received a fellowship from the French Ministère de l'Education Nationale. C.S. was supported by the Institut National de la Santé et de la Recherche Médicale and L.R. by the Emergence Program from the Ville de Paris.

1. Walton ME, Kennerley SW, Bannerman DM, Phillips PEM, Rushworth MFS (2006) Weighing up the benefits of work: Behavioral and neural analyses of effort-related decision making. *Neural Netw* 19(8):1302–1314.
2. Salamone JD, Correa M, Farrar A, Mingote SM (2007) Effort-related functions of nucleus accumbens dopamine and associated forebrain circuits. *Psychopharmacology (Berl)* 191(3):461–482.
3. Rangel A, Camerer C, Montague PR (2008) A framework for studying the neurobiology of value-based decision making. *Nat Rev Neurosci* 9(7):545–556.
4. Boksem MAS, Tops M (2008) Mental fatigue: Costs and benefits. *Brain Res Brain Res Rev* 59(1):125–139.
5. James W (1907) The energies of men. *Science* 25(635):321–332.
6. Gold JI, Shadlen MN (2007) The neural basis of decision making. *Annu Rev Neurosci* 30:535–574.
7. Heekeren HR, Marrett S, Ungerleider LG (2008) The neural systems that mediate human perceptual decision making. *Nat Rev Neurosci* 9(6):467–479.
8. Pessiglione M, et al. (2007) How the brain translates money into force: A neuroimaging study of subliminal motivation. *Science* 316(5826):904–906.
9. Schmidt L, Lebreton M, Cléry-Melin M-L, Daunizeau J, Pessiglione M (2012) Neural mechanisms underlying motivation of mental versus physical effort. *PLoS Biol* 10(2): e1001266.
10. Peyron R, Laurent B, García-Larrea L (2000) Functional imaging of brain responses to pain. A review and meta-analysis (2000). *Neurophysiol Clin* 30(5):263–288.
11. Friebel U, Eickhoff SB, Lotze M (2011) Coordinate-based meta-analysis of experimentally induced and chronic persistent neuropathic pain. *Neuroimage* 58(4): 1070–1080.
12. Krajbich I, Armel C, Rangel A (2010) Visual fixations and the computation and comparison of value in simple choice. *Nat Neurosci* 13(10):1292–1298.
13. Basten U, Biele G, Heekeren HR, Fiebach CJ (2010) How the brain integrates costs and benefits during decision making. *Proc Natl Acad Sci USA* 107(50):21767–21772.
14. Hunt LT, et al. (2012) Mechanisms underlying cortical activity during value-guided choice. *Nat Neurosci* 15(3):470–476, S1–S3.
15. Nybo L, Secher NH (2004) Cerebral perturbations provoked by prolonged exercise. *Prog Neurobiol* 72(4):223–261.
16. Subudhi AW, Miramon BR, Granger ME, Roach RC (2009) Frontal and motor cortex oxygenation during maximal exercise in normoxia and hypoxia. *J Appl Physiol* 106(4): 1153–1158.
17. Amann M, Dempsey JA (2008) Locomotor muscle fatigue modifies central motor drive in healthy humans and imposes a limitation to exercise performance. *J Physiol* 586(1): 161–173.
18. Logothetis NK (2008) What we can do and what we cannot do with fMRI. *Nature* 453 (7197):869–878.
19. Lee JH, et al. (2010) Global and local fMRI signals driven by neurons defined optogenetically by type and wiring. *Nature* 465(7299):788–792.
20. Gutschalk A, Hämäläinen MS, Melcher JR (2010) BOLD responses in human auditory cortex are more closely related to transient MEG responses than to sustained ones. *J Neurophysiol* 103(4):2015–2026.
21. Vartiainen J, Liljeström M, Koskinen M, Renvall H, Salmelin R (2011) Functional magnetic resonance imaging blood oxygenation level-dependent signal and magnetoencephalography evoked responses yield different neural functionality in reading. *J Neurosci* 31(3):1048–1058.
22. Rosa MJ, Daunizeau J, Friston KJ (2010) EEG-fMRI integration: A critical review of biophysical modeling and data analysis approaches. *J Integr Neurosci* 9(4):453–476.
23. Eickhoff SB, et al. (2010) Anatomical and functional connectivity of cytoarchitectonic areas within the human parietal operculum. *J Neurosci* 30(18):6409–6421.
24. Mohr C, Binkofski F, Erdmann C, Büchel C, Helmchen C (2005) The anterior cingulate cortex contains distinct areas dissociating external from self-administered painful stimulation: A parametric fMRI study. *Pain* 114(3):347–357.
25. Beckmann M, Johansen-Berg H, Rushworth MFS (2009) Connectivity-based parcellation of human cingulate cortex and its relation to functional specialization. *J Neurosci* 29(4):1175–1190.
26. Mazzola L, Isnard J, Peyron R, Mauguière F (2012) Stimulation of the human cortex and the experience of pain: Wilder Penfield's observations revisited. *Brain* 135(Pt 2): 631–640.
27. Craig ADB (2009) How do you feel—now? The anterior insula and human awareness. *Nat Rev Neurosci* 10(1):59–70.
28. Naqvi NH, Bechara A (2009) The hidden island of addiction: The insula. *Trends Neurosci* 32(1):56–67.
29. Jones CL, Ward J, Critchley HD (2010) The neuropsychological impact of insular cortex lesions. *J Neurol Neurosurg Psychiatry* 81(6):611–618.
30. Deecke L, Scheid P, Kornhuber HH (1969) Distribution of readiness potential, premotion positivity, and motor potential of the human cerebral cortex preceding voluntary finger movements. *Exp Brain Res* 7(2):158–168.
31. Colebatch JG (2007) Bereitschaftspotential and movement-related potentials: Origin, significance, and application in disorders of human movement. *Mov Disord* 22(5): 601–610.
32. Croxson PL, Walton ME, O'Reilly JX, Behrens TEJ, Rushworth MFS (2009) Effort-based cost-benefit valuation and the human brain. *J Neurosci* 29(14):4531–4541.
33. Kolling N, Behrens TEJ, Mars RB, Rushworth MFS (2012) Neural mechanisms of foraging. *Science* 336(6077):95–98.
34. Wager TD, et al. (2004) Placebo-induced changes in FMRI in the anticipation and experience of pain. *Science* 303(5661):1162–1167.
35. Tucker R (2009) The anticipatory regulation of performance: The physiological basis for pacing strategies and the development of a perception-based model for exercise performance. *Br J Sports Med* 43(6):392–400.
36. Noakes TD (2011) Time to move beyond a brainless exercise physiology: The evidence for complex regulation of human exercise performance. *Appl Physiol Nutr Metab* 36 (1):23–35.
37. Gandevia SC (2001) Spinal and supraspinal factors in human muscle fatigue. *Physiol Rev* 81(4):1725–1789.
38. Friston K, Mattout J, Trujillo-Barreto N, Ashburner J, Penny W (2007) Variational free energy and the Laplace approximation. *Neuroimage* 34(1):220–234.
39. Daunizeau J, Friston KJ, Kiebel SJ (2009) Variational Bayesian identification and prediction of stochastic nonlinear dynamic causal models. *Physica D* 238(21): 2089–2118.
40. Robert CP (2001) *The Bayesian Choice: From Decision Theoretic Foundations to Computational Implementation* (Springer, New York), 2nd Ed.
41. Stephan KE, Penny WD, Daunizeau J, Moran RJ, Friston KJ (2009) Bayesian model selection for group studies. *Neuroimage* 46(4):1004–1017.
42. Daunizeau J, et al. (2005) Assessing the relevance of fMRI-based prior in the EEG inverse problem: A Bayesian model comparison approach. *IEEE Trans Signal Process* 53(9):3461–3472.

Supporting Information

Meyniel et al. 10.1073/pnas.1211925110

SI Materials and Methods

Experimental Setting. Before scanning, participants were given written instructions to the task, which were repeated step by step orally. Subsequently, they were escorted inside the MRI or magnetoencephalography (MEG) scanning room and invited to find a comfortable body position that they could keep throughout the experiment. The only change was passing the power grip from one hand to the other between sessions. We used homemade power grips composed of two plastic cylinders compressing an air tube when squeezed. The tube led to the control room, where it was connected to a transducer converting air pressure into voltage. Thus, grip compression resulted in the generation of a differential voltage signal, linearly proportional to the force exerted. The signal was fed to the stimuli presentation PC via a signal conditioner (CED 1401; Cambridge Electronic Design) and read by a MATLAB program (MathWorks). Stimuli presentation was also programmed with MATLAB using Cogent 2000 (Wellcome Department of Imaging Neuroscience, London, UK).

fMRI Data Acquisition. Subject's head was constrained using foam and sand packs to limit movements. Functional echo-planar images (EPIs) were acquired with a T2*-weighted contrast on a 3-T scanner (Siemens Trio). Interleaved 2-mm slices separated by a 1.5-mm gap and oriented along a 30° tilted plane were acquired to cover the whole brain with a repetition time of 2 s. The first five scans were discarded to allow for equilibration effects. All preprocessing steps were performed using SPM8. Structural T1-weighted images were also acquired, coregistered with the mean EPI, segmented, and normalized to SPM standard Montreal Neurological Institute (MNI) T1 template. Normalized T1-images were averaged between subjects to localize group-level functional activations. EPIs were spatially realigned and normalized (using the same transformation as for structural images), and spatially smoothed with a 8-mm full-width at half-maximum Gaussian kernel.

MEG Data Acquisition. A whole-head MEG system comprising 151 axial gradiometers (CTF Systems) was used to sample brain activity at 1,250 Hz with online low-pass filter of 300 Hz. Head position was determined using marker coils at fiducial points (nasion, left and right ears). Ocular artifacts were marked manually and removed using the Gratton method with DataHandler (Cogimage, Centre de Recherche de l'Institut du Cerveau et de la Moelle Épinière, Paris, France). Data were imported in MATLAB and displayed using FieldTrip (Donders Institute, Nijmegen University, Nijmegen, The Netherlands). MEG signal was low-pass filtered offline at 30 Hz. Effort onsets and offsets were detected manually based on the electromyogram. A template mesh (8,196 tessels) and individual fiducials were used in SPM8 to compute a single shell head model and a lead field matrix per subject and session.

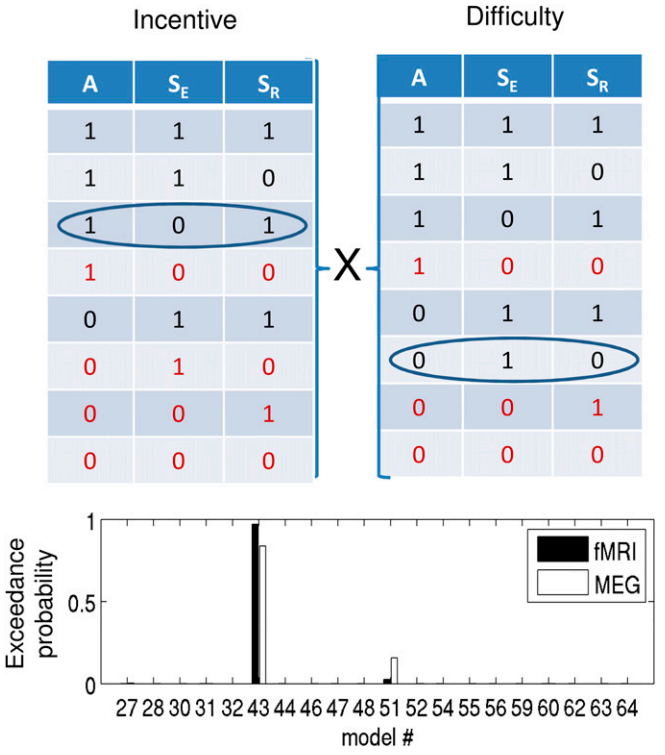

Fig. S1. Model comparison performed on behavioral data. The table illustrates all possible models obtained by varying the modulation of amplitude and slopes (A, S_e, and S_r) by monetary incentive (left columns) and/or task difficulty (right columns). Allowed (versus excluded) modulations are noted 1 (versus 0). "Allowed" means that there is a term for this modulation in the model. The red models are the combinations discarded a priori because they cannot reproduce the behavioral results. For instance, a model in which neither A or Se has an incentive term cannot reproduce Te modulation by incentives and therefore must be discarded. The surrounded combination corresponds to the model with the highest exceedance probability, calculated using Bayesian selection separately for fMRI and MEG subjects.

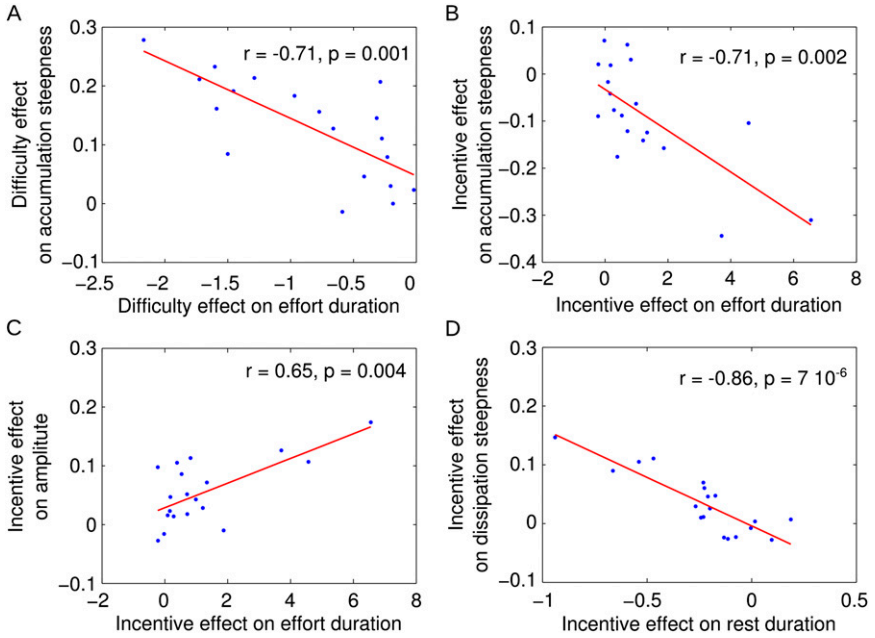

Fig. S2. Across-subject correlations between behavioral and computational effects of experimental factors (monetary incentive and task difficulty). Behavioral effects are as follows: shortened effort duration with higher task difficulty, prolonged effort duration with higher monetary incentive, and shortened rest duration with higher monetary incentive. Correlations were searched with all four computational effects that were found to explain these behavioral effects in MEG recordings. Computational effect refers to modulation of one parameter (accumulation steepness, dissipation steepness, or amplitude between bounds) of the signal reconstructed in our region of interest. Note that we use the term "steepness" and not "slope" because this power signal has no sign. The four computational effects are steeper accumulation with higher difficulty (*A*), slower accumulation with higher incentives (*B*), larger amplitude with higher incentives (*C*), and steeper dissipation with higher incentives (*D*). *R* values are Pearson ρ correlation coefficients; *P* values indicate the significance of robust-fit regressions (which underweight potential outliers).

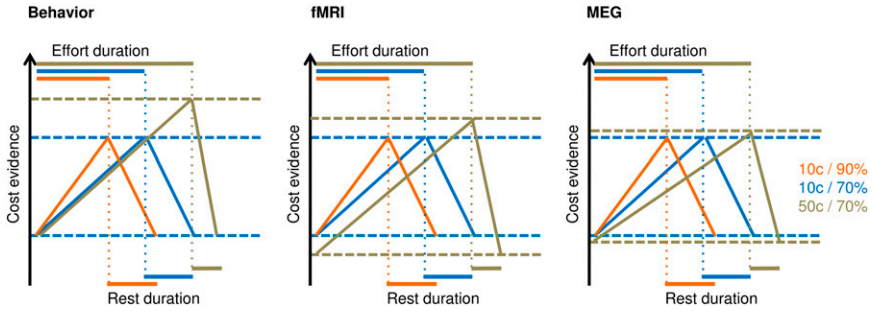

Fig. S3. Model refinement with fMRI and MEG findings. The diagrams illustrate how the experimental factors (monetary incentive and task difficulty) affect the accumulation of cost evidence. Compared with the blue line, the brown line shows the effect of increasing the incentive and the orange line the effect of increasing the difficulty. In the model that best explained the behavior (*Left*), the amplitude and dissipation slope are only impacted by incentives, whereas the accumulation slope is only impacted by difficulty. The fMRI results (*Center*) revealed that both the lower and upper bounds of the cost evidence signal encoded in brain activity are modulated by incentives. The MEG results (*Right*) revealed that the accumulation slope of this neural cost evidence is additionally impacted by incentives. Note that the three models produce the same pattern of effort and rest durations across conditions. In the final rightmost model, increasing the incentive (*i*) augments effort duration by inflating the amplitude and lowering the accumulation slope and (*ii*) reduces rest duration by accentuating the dissipation slope. In contrast, increasing the difficulty only shortens effort duration by enhancing the accumulation slope, without affecting the amplitude or dissipation slope.

Table S1. Brain regions parametrically modulated by the cost evidence signal in fMRI data analysis

Anatomical label	Peak *t*	Peak uncorrected *P*	Peak FWE *P*	Cluster FWE *P*	No. of voxels	Peak coordinates
Left posterior insula	5.825	0.000	0.011	0.006	226	[−40 −22 16]
Ventromedial thalamus	5.693	0.000	0.013	0.018	69	[2 −10 −4]
Right posterior insula	5.469	0.000	0.018	0.006	254	[42 −16 10]
Hypothalamus	4.819	0.000	0.053	0.031	36	[0 0 −20]
Fusiform gyrus	4.774	0.000	0.057	0.018	68	[22 −52 −10]
Cerebellum	4.422	0.000	0.100	0.041	24	[4 −46 −40]
Fusiform gyrus	4.234	0.001	0.132	0.038	27	[18 −70 −6]
Fusiform gyrus	4.227	0.001	0.133	0.035	30	[−10 −68 −4]

All clusters are listed that were observed using a voxel-wise threshold of $P < 0.001$, uncorrected, and a cluster-wise threshold of $P < 0.05$, family-wise error (FWE) corrected. The [*x y z*] peak coordinates in millimeters refer to the Montreal Neurological Institute (MNI) space.

Table S2. Brain regions parametrically modulated by the cost evidence signal when including the motor output (force) as a covariate in the GLM

Anatomical label	Peak *t*	Peak uncorrected *P*	Peak FWE *P*	Cluster FWE *P*	No. of voxels	Peak coordinates
Ventromedial thalamus	5.490	0.000	0.017	0.022	88	[2 −10 −4]
Right posterior insula	5.463	0.000	0.018	0.007	367	[42 −16 8]
Left posterior insula	5.410	0.000	0.019	0.008	286	[−42 −22 18]
Fusiform gyrus	4.661	0.000	0.064	0.005	616	[22 −52 −10]
Hypothalamus	4.578	0.000	0.073	0.033	59	[0 0 −20]
Cerebellum	4.540	0.000	0.078	0.032	61	[4 −48 −40]

All clusters are listed that were observed using a voxel-wise threshold of $P < 0.001$, uncorrected, and a cluster-wise threshold of $P < 0.05$, family-wise error (FWE) corrected. The [*x y z*] peak coordinates in millimeters refer to the Montreal Neurological Institute (MNI) space. The contrast tested is the cost evidence signal.